applied sciences

MDPI

Article

Switchable Chiral Metasurface for Terahertz Anomalous Reflection Based on Phase Change Material

Jiajia Chen [1], Xieyu Chen [1] and Zhen Tian [1,2,*]

[1] Center for Terahertz Waves and School of Precision Instrument and Optoelectronics Engineering, Key Laboratory of Optoelectronic Information Technology (Ministry of Education of China), Tianjin University, Tianjin 300072, China; chenjiajia522@tju.edu.cn (J.C.); chenxieyu@tju.edu.cn (X.C.)
[2] Department of Electrical and Computer Engineering, Georgia Tech Shenzhen Institute (GTSI), Tianjin University, Shenzhen 518067, China
* Correspondence: tianzhen@tju.edu.cn

Featured Application: This work provides a new strategy for the development of tunable terahertz chiral devices and will find applications in polarization-dependent fields.

Abstract: A switchable chiral metasurface based on a phase change material $Ge_2Sb_2Te_5$, which can switch between a right-handed circularly polarized mirror and a left-handed circularly polarized mirror, is theoretically discussed. When the conductivity of $Ge_2Sb_2Te_5$ σ is 0 S/m, the metasurface will reflect incident right-handed circularly polarized light and absorb incident left-handed circularly polarized light at 0.76 THz. As σ is set to 3×10^5 S/m, the response of the metasurface to circularly polarized light will be reversed. That is, it reflects the incident left-handed circularly polarized light and absorbs the incident right-handed circularly polarized light at 0.66 THz. The circular dichroism is from 76% to −64%. Then, we also study the performance of the mirror structure of the initial metasurface. By simulating the reflected spectra with different conductivities and the surface current distribution, the reason for the switchable function is clear. Moreover, the switchable chiral metasurface can be applied in spin-selective beam deflectors, which is proven by simulation. This work provides a new strategy for the development of tunable chiral devices.

Keywords: switchable; circular dichroism; anomalous reflection; terahertz wave

Citation: Chen, J.; Chen, X.; Tian, Z. Switchable Chiral Metasurface for Terahertz Anomalous Reflection Based on Phase Change Material. *Appl. Sci.* **2022**, *12*, 932. https://doi.org/10.3390/app12020932

Academic Editor: Saulius Juodkazis

Received: 1 December 2021
Accepted: 14 January 2022
Published: 17 January 2022

1. Introduction

Chirality is an inherent feature of chiral molecules. That is, an object cannot coincide with its mirror image through translation, turnover and other in-plane operations. Similar to our left and right hands, they mirror each other and cannot overlap. Chiral objects and their mirror images are called enantiomers. In the organic world, there are many chiral molecules, such as protein, DNA, sugar molecules, viruses, amino acids and liquid crystals, but there are few chiral structures in nature. Later, it is found that chiral materials can control the spin of electrons to a certain extent [1–3]. In addition, thanks to the development of metamaterials, the control of the spin of photons has been realized [4–10]. At present, the study of the interaction between circularly polarized light (CPL) and matter has been involved in many wavebands, such as microwave [11], terahertz [12], infrared [13] and visible [14]. It is well known that chiral metamaterials show different electromagnetic responses such as asymmetric transmission (AT) and circular dichroism (CD) when they interact with CPL with different spins. In other words, chiral metamaterials have selective transmission, reflection and absorption of incident CPL with different spins.

In recent years, metamaterials with spin selectivity have played a very important role in many fields. For example, spin-selective beam deflectors [15], polarization-sensitive chiral circularly polarized light detectors [16], circularly polarized light multiplexed holograms [17] and spin- and wavelength-sensitive gray imaging [18]. However, the optical

effect of metamaterials is difficult to change after manufacturing, which limits the practical application of functional metamaterials. Hence, actively tunable metamaterials are gaining increasing attention. At present, there are two design methods that can make metamaterials have the property of active regulation. The first method is to change the geometry of metamaterials. Hu Tao et al. proposed a reconfigurable anisotropic metamaterial at terahertz frequency, which can bend the structure through thermal stimulation to change the structural response [19]. Yuan Hsing Fu et al. designed a micromechanically reconfigurable metamaterial. Dynamic tuning can be realized by changing the coupling distance between cells through bidirectional micromechanical actuators [20]. The second method is to add controllable materials such as silicon, graphene and phase change materials into metamaterials. Lei Kang et al. presented a nonlinear chiral meta-mirror based on silicon, which can be used for an all-optical picosecond optical polarization switch. The chiral optical response of the structure is dynamically adjusted by the change of carriers in silicon by pump light [21]. Chuanchuan Ding et al. proposed an absorber integrating a periodic $Ge_2Sb_2Te_5$ (GST) resonator. Through the phase transition of the GST resonator from an amorphous state to a crystalline state, a change in CD intensity in the range of 0.03 to 0.75 can be realized [22].

In contrast to the past, some researchers have shifted their attention from tuning the chiral response intensity to switching the chiral response. Meng Liu et al. took advantage of vanadium dioxide (VO_2) to change the chirality of metamaterial resonators and realized a change in CD intensity from −75% to +55% [23]. Xiaoqing Luo et al. proposed a dynamically reversible chiral metamaterial by combining vanadium dioxide and Babinet's principle, which can achieve a reversible CD tuning range of ±0.5 at 0.97 THz [24]. Yongkai Wang et al. realized a reversible chiral response in the terahertz band by making use of achiral dielectric and graphene bands. Chiral response switching can be realized by reversing the Fermi level of the graphene band [25]. From the perspective of practical application, the design of a dynamically reversible metamaterial with strong circular dichroism is more in line with the application requirements.

Here, we theoretically investigate a switchable chiral metasurface based on a phase change material GST, which can switch between a right-handed circularly polarized (RCP) mirror and a left-handed circularly polarized (LCP) mirror. The metasurface is composed of asymmetric split-ring resonators (ASRRs) arranged periodically. The simulated results show that when the conductivity of GST σ is equal to 0 S/m, ASRR_1 will reflect incident right-handed circularly polarized light (RCPL) and absorb incident left-handed circularly polarized light (LCPL) at 0.76 THz. As σ rises to 3×10^5 S/m, the response of ASRR_1 to circularly polarized light will be reversed. That is, it reflects the incident LCPL and absorbs the incident RCPL at 0.66 THz. In addition, we also simulate ASRR_2, the mirror structure of ASRR_1. Then, the effect of conductivity on the properties of ASRR_1 was also studied. In addition, the physical principle of ASRR_1 was explained. Finally, we arrange ASRR_1 into a phase continuous metasurface. Before and after the GST phase transition, it can anomalously reflect the incident LCPL and RCPL out of the whole metasurface at different angles.

2. Materials and Methods

The performance of the switchable metasurface was numerically simulated by a commercial full-wave numerical software computer simulation technology (CST) Microwave Studio. The frequency-domain solver is selected as the simulated method. On a single periodic structural element, the boundary conditions in the x and y directions are set as unit cells, and the boundary condition in the z direction is open. When x- and y-polarized plane waves are incident, due to the existence of polarization conversion, we obtain the following reflection coefficients of linearly polarized light: r_{xx}, r_{yx}, r_{yy} and r_{xy}. Then, the reflection coefficient of CPL can be obtained by Equation (1). Here, x, y, r and l in the subscript represent x-polarized light, y-polarized light, right-handed circularly polarized light and left-handed circularly polarized light, respectively. R_{ij} represents the reflection

coefficient of *i*-polarized light reflected by the structure under the incidence of *j*-polarized light, $i, j \in \{x, y, r, l\}$. It should be pointed out that we will observe circularly polarized light facing the propagation direction of electromagnetic waves. At a fixed position, if the polarization direction rotates clockwise with time, it is RCPL; in contrast, it is LCPL.

$$\begin{pmatrix} R_{rr} & R_{rl} \\ R_{lr} & R_{ll} \end{pmatrix} = \frac{1}{2} \begin{pmatrix} R_{xx} - R_{yy} + i(R_{xy} + R_{yx}) & R_{xx} + R_{yy} - i(R_{xy} - R_{yx}) \\ R_{xx} + R_{yy} + i(R_{xy} - R_{yx}) & R_{xx} - R_{yy} - i(R_{xy} + R_{yx}) \end{pmatrix} \quad (1)$$

Figure 1a,b shows a schematic diagram of the unit structure of ASRR_1. Here, a continuous uniform metal film *rr* with a thickness of 200 nm is used as the reflecting layer. The top of each unit is an ASRR composed of metal and phase change material GST. A 50 μm thick polyimide (PI) dielectric layer separates the bottom metal film from the top ASRR. In the simulation, the metal structures were made of aluminum (Al) with a conductivity of 3.56×10^7 S/m. The dielectric constant and loss tangent of PI are 2.93 and 0.044, respectively. The thickness, outer radius R and linewidth w of ASRR_1 are 200 nm, 65 μm and 20 μm, respectively. The angle of gaps α and β are 20° and 40°. φ is the angle at which ASRR_1 rotates around the z-axis. The period of the unit structure P is 160 μm. Figure 1c shows the schematic of the electromagnetic responses of a gradient chiral metamirror, which is obtained by arranging ASRR_1 into a phase continuous metasurface.

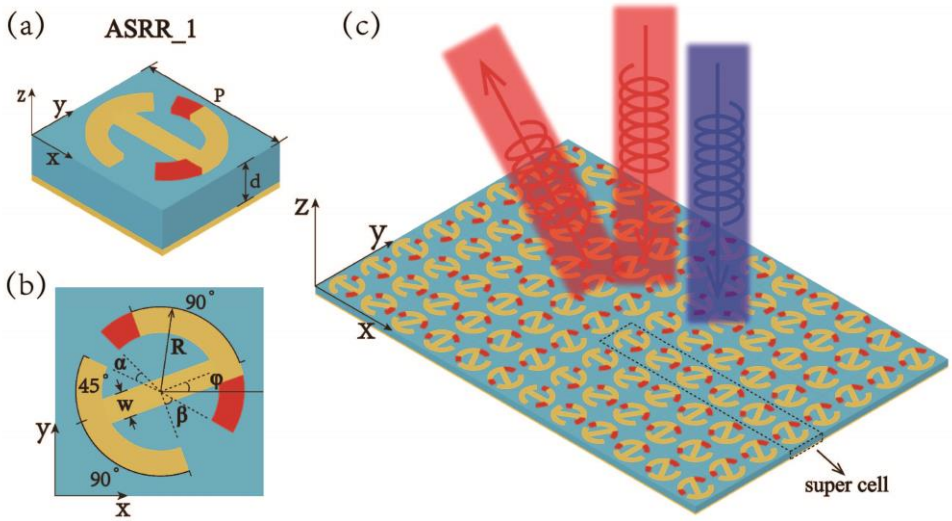

Figure 1. Schematic of (**a**) the electromagnetic responses of a gradient chiral metamirror and (**b**,**c**) the structure of a unit cell.

3. Results

First, we simulate the reflection spectra of ASRR_1 and ASRR_2, which are mirror images of each other. Figure 2a–d shows the unit structure diagram and the reflection spectrum results of ASRR_1. As shown in Figure 2b, when the conductivity of GST σ is 0 S/m, ASRR_1 will efficiently absorb the incident LCPL at a frequency of 0.76 THz, while it will strongly reflect the incident RCPL. That is, $R_{rr} = 0.76$ and $R_{ll} = 0$. At this time, ASRR_1 is called RCP mirror. As σ rises to 3×10^5 S/m, it can be seen from Figure 2c that ASRR_1 is switched to the LCP mirror. That is, it can efficiently absorb the incident RCPL and strongly reflect the incident LCPL. The reflectivity is $R_{rr} = 0.02$ and $R_{ll} = 0.66$. Since GST after the phase transition increases the electrical length of the whole structure, the working frequency of ASRR_1 shifts red to 0.66 THz. The quantitative calculation of circular dichroism is CD = $R_{rr} - R_{ll}$. In Figure 2d, before the phase transition, the circular dichroism of ASRR_1 is CD = 76%. After the phase transition, the circular dichroism of ASRR_1 is CD = −64%. This also shows that switching between the RCP mirror and LCP mirror is realized by using the phase transition property of GST. Figure 2e–h shows the unit structure diagram and the reflection spectrum results of ASRR_2. As ASRR_2 and ASRR_1

are mirror image relationships in structure, their reflection spectrum and CD spectrum also show a reversal effect. That is, ASRR_2 is an LCP mirror before the GST phase transition and will switch to an RCP mirror after the GST phase transition. Its circular dichroism changes from CD = −76% to CD = 64%.

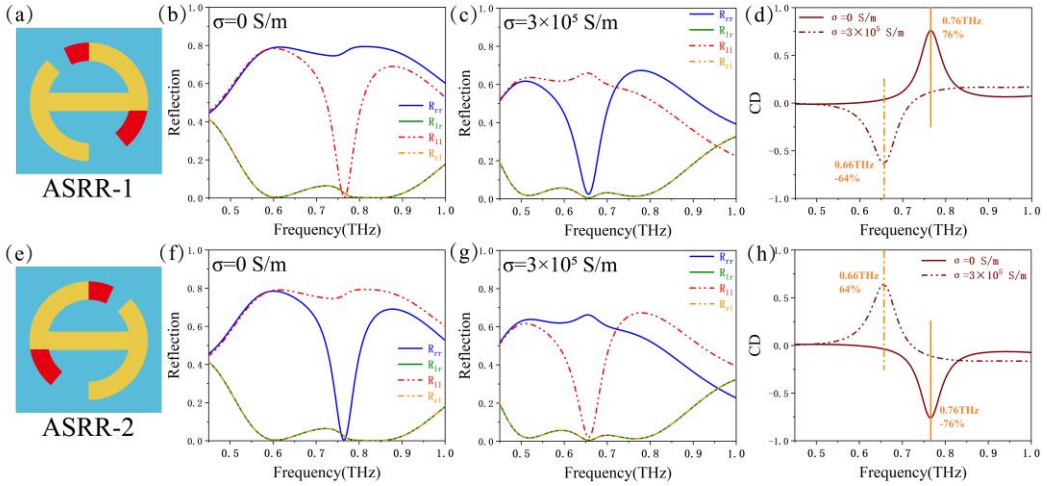

Figure 2. Schematic diagram of structural units, reflection spectrum and circular dichroism curve spectrum of (**a**–**d**) ASRR_1 and (**e**–**h**) ASRR_2.

Next, there are several reflection spectra of ASRR_1 with obvious changes under different conductivities in Figure 3. We have explained that the reflection effects of ASRR_1 and ASRR_2, which are mirror structures to each other, are reversed to each other in Figure 2. Therefore, only the simulation results of ASRR_1 will be discussed in future research. With increasing conductivity, the reflection valley of LCPL at 0.76 THz is gradually passivated, and the reflectivity increases. Moreover, the reflectivity difference between the RCPL and LCPL will also gradually decrease. As $\sigma = 6 \times 10^4$ S/m, the reflection valley of LCPL basically disappears. At this time, reflection valley of RCPL appeared at 0.66 THz. Moreover, the reflection valley of RCPL will gradually sharpen, and the reflectivity will decrease with increasing conductivity. At the same time, the reflectivity difference between the RCPL and LCPL also increases. When σ is 3×10^5 S/m, ASRR_1 completes the switching from the RCP mirror to the LCP mirror.

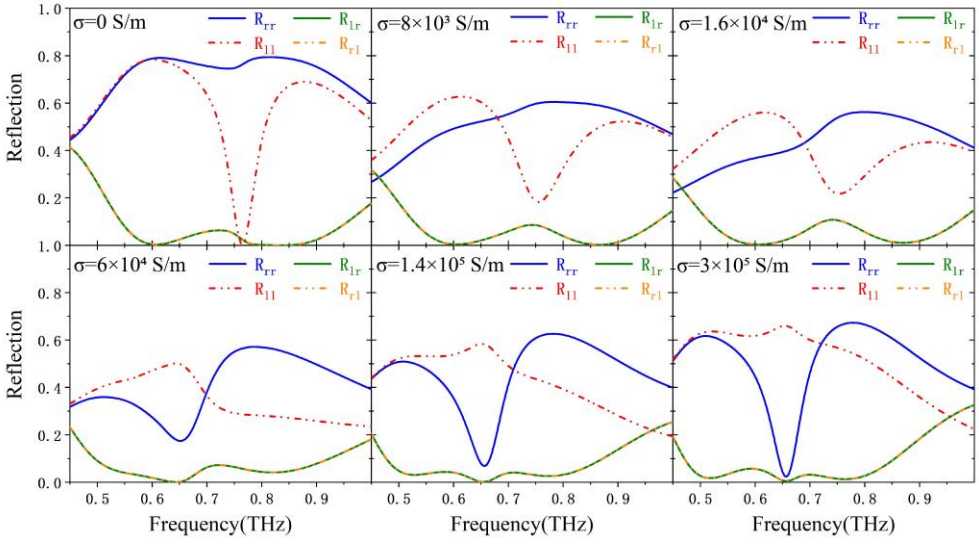

Figure 3. Reflection spectra of ASRR_1 with different conductivities of GST.

To explain the physical mechanism of this switchable chiral metasurface, the surface current distribution of ASRR_1 under different conductivities is simulated, as shown in Figure 4. Here, we mark the current oscillation direction along the two arms of ASRR_1 with a white arrow. When the conductivity of GST is 0 S/m, ASRR_1 shows the effect of absorption of LCPL and reflection of RCPL at 0.76 THz. As seen from Figure 4a, the surface current oscillates in a single direction on the two arms, which shows that the incident LCPL excites a magnetic dipole resonance in ASRR_1. This resonant mode can bind the incident electromagnetic wave energy inside the structure, and the lossy PI layer will slowly absorb the energy. Therefore, LCPL is highly absorbed after incident on ASRR_1. In Figure 4b, the surface current oscillates in different directions along the two arms of the resonant ring, indicating that the incident RCPL excites an electric dipole with low loss in ASRR_1. Thus, the metasurface at this time presents the performance of reflecting RCP incident light. As σ is 3×10^5 S/m, ASRR_1 shows the effect of reflecting LCPL and absorbing RCPL at 0.66 THz. According to the current distribution in Figure 4c, the incident LCPL excited in the structure is an electric dipole; thus, LCPL is reflected. Similarly, by analyzing Figure 4d, it can be seen that the magnetic dipole that will cause high absorption is excited after the RCPL is incident on ASRR_1. Through the analysis, we can clearly understand that the different resonance modes excited by incidence lead to the different responses of the chiral metasurface to circularly polarized light with different spins under different conductivities.

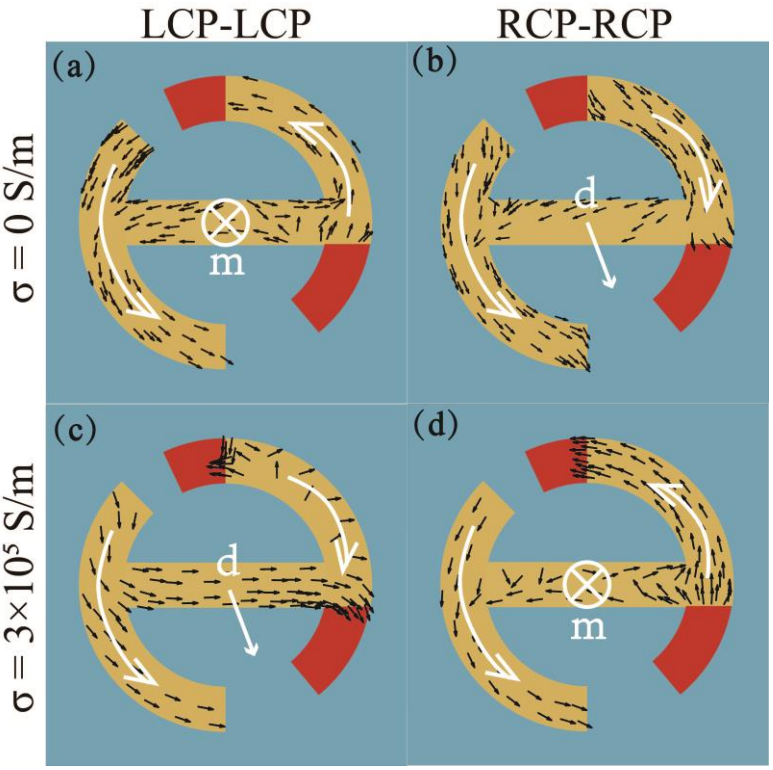

Figure 4. The physical mechanism of the switchable chiral metasurface. The surface current distribution of ASRR_1 with conductivities of (**a**,**b**) 0 S/m and (**c**,**d**) 3×10^5 S/m when LCP and RCP are incident.

According to the Pancharatnam–Berry phase [26], when a structure rotates φ around the z-axis, the phase of the reflected light will change by 2φ, while the amplitude of the reflected light remains unchanged. Then, the reflection spectrum of ASRR_1 with different orientations φ is simulated. As shown in Figure 5a, RCPL is incident to ASRR_1. The conductivity of GST is σ = 0 S/m. Regardless of the value of φ, the reflection remains almost unchanged and approximately equals 0.76. When φ changes from 0 to π at an interval of π/18, the phase of reflected RCPL changes between −π and π, that is, the phase

change range is 2π. The operating frequency is 0.76 THz. Figure 5b shows that ASRR_1 with σ = 3 × 10^5 S/m is irradiated by LCPL. Similarly, the amplitude of reflected LCPL, which is approximately 0.66, will not change with different φ. The phase of reflected LCPL depends on 2φ and changes in the range of 2π. The operating frequency here is 0.66 THz.

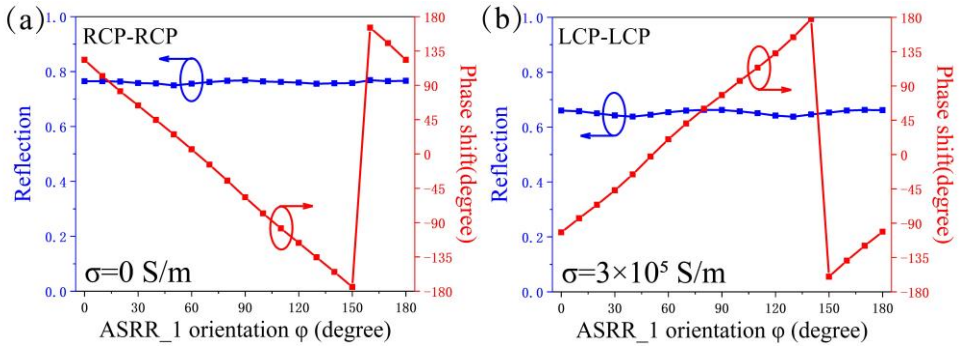

Figure 5. The reflection amplitude and phase changes of ASRR_1 with conductivities of (**a**) 0 S/m and (**b**) 3 × 10^5 S/m with different orientations θ around the z-axis.

In the generalized Snell's law, we can control the direction of the emitted light by designing a linear varied phase shift $\phi(x)$ along the surface of a metasurface. For reflected light, the equation of generalized Snell's law is defined as [27]:

$$n_r \sin\theta_r = n_i \sin\theta_i + \frac{c}{2\pi f}\frac{d\phi(x)}{dx} \quad (2)$$

where θ_r and θ_i represent the reflection angle and incident angle, respectively; n_r and n_i represent the refractive indices of the output and input media, which are equal to 1; c is the speed of light in vacuum; f corresponds to the operating frequency of the metasurface; and $d\phi(x)/dx$ stands for a constant phase gradient. PB phase is a method to accurately control $\phi(x)$. That is $\phi(x) = \pm 2\varphi$ [28]. φ here is the rotation angle of ASRR_1 around the z-axis we mentioned above. The sign plus or minus is determined by RCPL and LCPL. As seen from Figure 5, ASRR_1 can change the phase of its reflected light by rotating around the z-axis, and the phase size can cover the whole phase period 2π. Therefore, we chose six different rotation angles: 0, π/6, π/3, π/2, 2π/3 and 5π/6. The six small units are arranged in a row to form a superperiodic unit cell and thus a chiral metasurface with linear phase change that covers the whole 2π range. Part of the structure of the chiral metasurface is shown in Figure 1c. The period in the x direction is P_x = 960 μm, and the period in the y direction is P_y = 160 μm. Similarly, we use the simulation software CST to simulate the reflected field distribution of the metasurface.

Figure 6a,b show the results of LCPL and RCPL incident on the chiral metasurface with a conductivity of 0 S/m, respectively. It can be clearly seen that the RCPL incident vertically has obvious deflection after being reflected by the metasurface, that is, anomalous reflection. Because the metasurface under this conductivity will efficiently absorb the incident LCPL, the reflected electric field is almost invisible. In addition, we simulate the reflected electric field with a conductivity of 3 × 10^5 S/m. As shown in Figure 6c,d, the results correspond to the LCP incidence and RCP incidence, respectively. When LCPL is incident vertically, it will be anomalously reflected off the chiral metasurface. However, the incident RCPL will be absorbed. The uniform wavefront in Figure 6b,c shows that the amplitudes of circularly polarized light reflected by the six structures are almost equal, which is consistent with the results obtained in Figure 5. Comparing the two figures, we can see that the angles of the chiral metasurface anomalously reflected under the two conductivities are different. There are two reasons for the difference: the first is the different working frequencies, and the second is the reflected light with different spins. Regardless of the conductivity, the

linear phase distribution of the metasurface takes $\pi/3$ as the gradient. Thus, according to Equation (2), the two deflection angles are 24.3° and −28.3°.

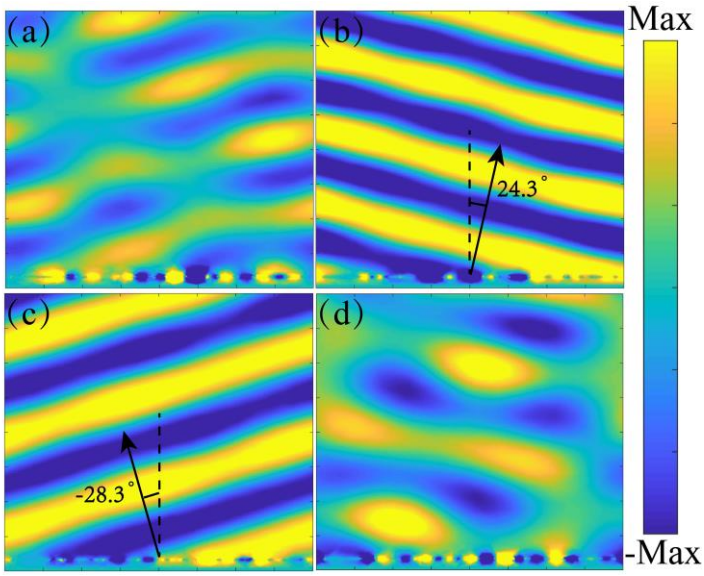

Figure 6. Simulated electric distributions of anomalous reflection with conductivities of (**a**,**b**) 0 S/m and (**c**,**d**) 3×10^5 S/m.

4. Conclusions

In conclusion, we proposed a switchable chiral metasurface that can switch between the RCP mirror and LCP mirror by making use of the phase transition of GST. As σ = 0 S/m, ASRR_1 will reflect 76% incident RCPL and perfectly absorb incident LCPL at 0.76 THz. When σ is equal to 3×10^5 S/m, the response of ASRR_1 to circularly polarized light will be reversed. It reflects the incident LCPL and absorbs the incident RCPL at 0.66 THz. Moreover, the performance of ASRR_2, the mirror structure of ASRR_1, is also investigated. Then, we simulate the reflected spectra with different inductivities and the surface current distribution of ASRR_1 to understand the root cause of switching. Finally, we demonstrate that this chiral metasurface can realize anomalous reflection by using the geometric phase and generalized Snell's law. Consequently, this work offers a new idea for realizing active and tunable optical chirality and will find applications in polarization-dependent fields.

Author Contributions: Conceptualization, Z.T.; validation, J.C. and X.C.; formal analysis, Z.T., J.C. and X.C.; investigation, J.C. and X.C.; writing—original draft preparation, J.C.; writing—review and editing, Z.T.; supervision, Z.T.; project administration, Z.T.; funding acquisition, Z.T. All authors have read and agreed to the published version of the manuscript.

Funding: This work was supported by the National Key Research and Development Program of China (2017YFA0701004), Tianjin Municipal Fund for Distinguished Young Scholars (Grant No. 20JCJQJC00190), and Key Fund of Shenzhen Natural Science Foundation (Grant No. JCYJ20200109150212515).

Institutional Review Board Statement: Not applicable.

Informed Consent Statement: Not applicable.

Data Availability Statement: The data presented in this study are available on request from the corresponding author.

Conflicts of Interest: The authors declare no conflict of interest.

References

1. Fontanesi, C.; Capua, E.; Paltiel, Y.; Waldeck, D.H.; Naaman, R. Spin-Dependent Processes Measured without a Permanent Magnet. *Adv. Mater.* **2018**, *30*, 1707390. [CrossRef]
2. Mishra, S.; Kumar, A.; Venkatesan, M.; Pigani, L.; Pasquali, L.; Fontanesi, C. Exchange Interactions Drive Supramolecular Chiral Induction in Polyaniline. *Small Methods* **2020**, *4*, 2000617. [CrossRef]
3. Mishra, S.; Pasquali, L.; Fontanesi, C. Spin control using chiral templated nickel. *Appl. Phys. Lett.* **2021**, *118*, 224001. [CrossRef]
4. Schwanecke, A.S.; Fedotov, V.A.; Khardikov, V.V.; Prosvirnin, S.L.; Chen, Y.; Zheludev, N.I. Nanostructured Metal Film with Asymmetric Optical Transmission. *Nano Lett.* **2008**, *8*, 2940–2943. [CrossRef] [PubMed]
5. Zhukovsky, K.V.; Novitsky, A.V.; Galynsky, V.M. Elliptical dichroism: Operating principle of planar chiral metamaterials. *Opt. Lett.* **2009**, *34*, 1988–1990. [CrossRef] [PubMed]
6. Plum, E.; Fedotov, V.A.; Zheledev, N.I. Extrinsic electromagnetic chirality in metamaterials. *J. Opt.* **2009**, *11*, 074009. [CrossRef]
7. Wu, L.; Yang, Z.Y.; Cheng, Y.Z.; Zhao, M.; Gong, R.Z.; Zheng, Y.; Duan, J.; Yuan, X.H. Giant asymmetric transmission of circular polarization in layer-by-layer chiral metamaterials. *Appl. Phys. Lett.* **2013**, *103*, 021903. [CrossRef]
8. Plum, E.; Zhenludev, N.I. Chiral mirrors. *Appl. Phys. Lett.* **2015**, *106*, 221901. [CrossRef]
9. Long, F.; Yu, S.X.; Kou, N.; Zhang, C.; Ding, Z.; Zhang, Z.P. Wideband and high-efficiency planar chiral structure design for asymmetric transmission and linear polarization conversion. *J. Appl. Phys.* **2020**, *127*, 023104. [CrossRef]
10. Liu, C.J.; Huang, Y.Y.; Hu, F.R.; Yiwen, E.; Dong, X.X.; Yang, Y.; Jin, Y.P.; Xu, X.L. Giant Asymmetric Transmission and Circular Dichroism with Angular Tunability in Chiral Terahertz Metamaterials. *Ann. Phys.* **2020**, *532*, 1900398. [CrossRef]
11. Jing, L.Q.; Wang, Z.J.; Yang, Y.H.; Zheng, B.; Liu, Y.M.; Chen, H.S. Chiral metamirrors for broadband spin-selective absorption. *Appl. Phys. Lett.* **2017**, *110*, 231103. [CrossRef]
12. Yang, S.Y.; Liu, Z.; Hu, S.; Jin, A.Z.; Yang, H.F.; Zhang, S.; Li, J.J.; Gu, C.Z. Spin-Selective Transmission in Chiral Folded Metasurfaces. *Nano Lett.* **2020**, *19*, 3432–3439. [CrossRef]
13. Mao, L.B.; Liu, K.; Zhang, S.; Cao, T. Extrinsically 2D-Chiral Metamirror in Near-Infrared Region. *ACS Photonics* **2020**, *7*, 375–383. [CrossRef]
14. Rana, A.S.; Kim, I.; Ansari, M.A.; Anwar, M.S.; Saleem, M.; Tauqeer, T.; Danner, A.; Zubair, M.; Mehmood, M.Q.; Rho, J. Planar Achiral Metasurfaces-Induced Anomalous Chiroptical Effect of Optical Spin Isolation. *ACS Appl. Mater. Interfaces* **2020**, *12*, 48899–48909. [CrossRef] [PubMed]
15. Jing, L.Q.; Wang, Z.J.; Maturi, R.; Zheng, B.; Wang, H.P.; Yang, Y.H.; Shen, L.; Hao, R.; Yin, W.Y.; Li, E.P.; et al. Gradient Chiral Metamirrors for Spin-Selective Anomalous Reflection. *Laser Photonics Rev.* **2017**, *11*, 1700115. [CrossRef]
16. Li, W.; Coppens, Z.J.; Besteiro, L.V.; Wang, W.Y.; Govorov, A.O.; Valentine, J. Circularly polarized light detection with hot electrons in chiral plasmonic metamaterials. *Nat. Commun.* **2015**, *6*, 8379. [CrossRef]
17. Wang, Q.; Plum, E.; Yang, Q.L.; Zhang, X.Q.; Xu, Q.; Xu, Y.H.; Han, J.G.; Zhang, W.L. Reflective chiral meta-holography: Multiplexing holograms for circularly polarized waves. *Light Sci. Appl.* **2018**, *7*, 25. [CrossRef]
18. Li, Z.C.; Liu, W.W.; Cheng, H.; Choi, D.Y.; Chen, S.Q.; Tian, J.G. Spin-Selective Full-Dimensional Manipulation of Optical Waves with Chiral Mirror. *Adv. Mater.* **2020**, *32*, 1907983. [CrossRef]
19. Tao, H.; Strikwerda, A.C.; Fan, K.; Padilla, W.J.; Zhang, X.; Averitt, R.D. Reconfigurable Terahertz Metamaterials. *Phys. Rev. Lett.* **2009**, *103*, 147401. [CrossRef]
20. Fu, Y.H.; Liu, A.Q.; Zhu, W.M.; Zhang, X.M.; Tsai, D.P.; Zhang, J.B.; Mei, T.; Tao, J.F.; Guo, H.C.; Zhang, X.H.; et al. A Micromachined Reconfigurable Metamaterial via Reconfiguration of Asymmetric Split-Ring Resonators. *Adv. Funct. Mater.* **2011**, *21*, 3589–3594. [CrossRef]
21. Kang, L.; Wang, C.Y.; Guo, X.X.; Ni, X.J.; Liu, Z.W.; Werner, D.H. Nonlinear Chiral Meta-Mirrors: Enabling Technology for Ultrafast Switching of Light Polarization. *Nano Lett.* **2020**, *20*, 2047–2055. [CrossRef]
22. Ding, C.C.; Rui, G.H.; Gu, B.; Zhan, Q.W.; Cui, Y.P. Phase-change metasurface with tunable and switchable circular dichroism. *Opt. Lett.* **2021**, *46*, 2525–2528. [CrossRef]
23. Liu, M.; Plum, E.; Li, H.; Duan, S.Y.; Li, S.X.; Xu, Q.; Zhang, X.Q.; Zhang, C.H.; Zou, C.W.; Jin, B.B.; et al. Switchable Chiral Mirrors. *Adv. Opt. Mater.* **2020**, *8*, 2000247. [CrossRef]
24. Luo, X.Q.; Hu, F.R.; Li, G.Y. Dynamically reversible and strong circular dichroism based on Babinet-invertible chiral metasurfaces. *Opt. Lett.* **2021**, *46*, 1309–1312. [CrossRef] [PubMed]
25. Wang, Y.K.; Wang, Q.J.; Wang, Q.Y.; Wang, Y.Y.; Li, Z.D.; Lan, X.; Dong, J.; Gao, W.; Han, Q.Y.; Zhang, Z.Y. Dynamically adjustable-induced THz circular dichroism and biosensing application of symmetric silicon-graphene-metal composite nanostructures. *Opt. Express* **2021**, *29*, 8087–8097. [CrossRef] [PubMed]
26. Muehlenbernd, H.; Georgi, P.; Pholchai, N.; Huang, L.L.; Li, G.X.; Zhang, S.; Zentgraf, T. Amplitude- and Phase-Controlled Surface Plasmon Polariton Excitation with Metasurfaces. *ACS Photonics* **2016**, *3*, 124–129. [CrossRef]
27. Larouche, S.; Smith, D.R. Reconciliation of generalized refraction with diffraction theory. *Opt. Lett.* **2012**, *37*, 2391. [CrossRef]
28. Chen, X.Z.; Huang, L.L.; Muhlenbernd, H.; Li, G.X.; Bai, B.F.; Tan, Q.F.; Jin, G.F.; Qiu, C.W.; Zhang, S.; Zentgraf, T. Dual-polarity plasmonic metalens for visible light. *Nat. Commun.* **2012**, *3*, 1198. [CrossRef]